PHYSICAL REVIEW B VOLUME 46, NUMBER 9 1 SEPTEMBER 1992-I

Phase selection in undercooled quasicrystal-forming Al-Mn alloy melts

D. M. Herlach, F. Gillessen, and T. Volkmann
Deutsche Forschungsanstalt für Luft- und Raumfahrt, Institut für Raumsimulation, D-5000 Köln 90, Germany

M. Wollgarten and K. Urban
Forschungszentrum Jülich, Institut für Festkörperforschung, D-5170 Jülich, Germany

(Received 18 February 1992)

Small droplets in size of 20–1000 μm of Al-Mn alloys have been undercooled by containerless solidification during free fall in a drop tube or by melt atomization. The as-solidified droplets were analyzed with respect to the phases formed from the undercooled melt by electron microscopy, x-ray diffraction, and differential thermal analysis. Depending on the droplet size, various phases have been identified ranging from supersaturated Al_{SS}, intermetallic Al_6Mn, to quasicrystalline phases. The observed phase formation was interpreted in terms of nucleation, crystal growth, and transformation kinetics on the basis of current theories. This analysis gives a comprehensive description of phase formation in undercooled Al-Mn alloys in agreement with the experimental findings.

I. INTRODUCTION

Quasicrystalline phases have been the subject of extensive investigations since the detection of a phase with fivefold symmetry in a rapidly quenched Al-Mn alloy by Shechtman *et al.*[1] The two most important quasicrystalline phases are the icosahedral or *I* phase, which is quasiperiodic in three dimensions,[1] and the decagonal or *T* phase, which is quasiperiodic in two dimensions and periodic in the third.[2] With a few exceptions,[3–5] quasicrystalline phases have been found to be metastable.

Solidification of a metastable phase from the liquid state requires an undercooling of the melt below the virtual melting point of the metastable phase prior to solidification. Only under such conditions is a driving force for nucleation of the respective phase available. Classical nucleation theory[6] describes the activation energy for nucleation as a function of the interface energy σ, which gives rise to an energy barrier against phase transformation. The free-energy difference between the undercooled liquid and solid state, ΔG_v, acts as the driving force for phase transformation. The latter can be determined from experimental data on the specific heat in the undercooled liquid and solid states. More recently, the specific heat of Al-Cu-V alloys has been measured as a function of temperature both for the liquid and quasicrystalline solid states.[7]

The interface energy is more difficult to determine. The interfacial energy between nucleus and melt has been described within a negentropic model by Spaepen.[8] This model is based on the assumption that the sort-range order in the interface is tetrahedral. A tetrahedron is the basic element of an icosahedron, which consists of 20 tetrahedrons. As already pointed out by Frank,[9] the short-range order within undercooled melts should be icosahedral in nature, as confirmed by computer-simulation experiments on Lennard-Jones liquids.[10] This in turn implies that the interfacial energy will be smallest for icosahedral nuclei within an undercooled melt of icosahedral-like short-range order.[11] Therefore homogeneous nucleation of the icosahedral phase should be possible even at moderate undercooling, in contrast to nucleation of crystalline phases. In the latter case, a higher nucleation barrier is expected as a result of a higher interfacial energy. Moreover, nucleation of the crystalline phase requires a breaking of the icosahedral symmetry of the undercooled melt, if present, prior to crystallization, since its fivefold symmetry is incompatible with the long-range translational symmetry of a lattice.

Previous experimental investigations indicate homogeneous nucleation of quasicrystalline phases of Al-Mn provided conditions for heterogeneous nucleation are unfavorable. This is the case in processing of small droplets in the containerless state under high pure environment.[12–14] These experiments show a sequence of phase formation as a function of processing conditions different to that obtained by rapid quenching Al-Mn melts.[15–18]

In the present work, we report drop-tube and atomization experiments in which droplets of Al-Mn alloys have been prepared in sizes of 20–1000 μm. The phases formed in the droplets have been analyzed by transmission electron microscopy (TEM), x-ray diffraction, and differential scanning calorimetry (DSC). A contour map is developed by plotting the mass fractions of phases solidified as a function of droplet size. Since the droplet size correlates directly to the cooling rate of the molten droplets, these investigations allow a systematic analysis of the kinetics of phase formation in the undercooled Al-Mn samples. The results are interpreted within current theories of nucleation, crystal growth, and transformation kinetics and give a comprehensive description of the formation of crystalline and quasicrystalline phases in undercooled Al-Mn melts. These investigations on the undercooled liquid state are analogous to those recently reported on the crystallization behavior from the solid state of rapidly quenched alloys of the same system.[19]

II. EXPERIMENT

Alloy ingots of $Al_{88}Mn_{12}$ were prepared by remelting the constituents, with a purity of 99.999% (Al) and

99.97% (Mn), in an arc furnace under a purified Ar atmosphere. The as-prepared ingots were used for drop-tube and melt-atomization experiments. The drop tube consists of a glass tube of 2.5 m length, which can be evacuated to a pressure of 1×10^{-7} mbar before backfilling it with purified helium gas. Alloy samples were placed into crucibles of glassy carbon and melted inductively. The temperature of the melt was measured by a two-colour pyrometer with a relative accuracy of better than ±5 K. Subsequently, the melt was dispersed as small droplets into the drop tube by forcing the melt through a thin nozzle at the lower end of the crucible. Droplets in size ranging from 100 to 1000 μm were obtained in this way. Further details of the drop tube are given elsewhere.[20]

The cooling rate of the liquid droplets during free fall was estimated by thermal-balance calculations. Assuming Newtonian conditions, the cooling rate $\dot{T}=dT/dt$ of freely falling droplets of diameter d is given by

$$\dot{T}=\frac{6}{\rho C_p d}[h_m(T-T_R)+\sigma_{SB}\varepsilon(T^4-T_R^4)] , \quad (1)$$

where h_m is the heat-transfer coefficient for forced convection from a sphere,[21] ρ the density of the sample material, T_R the room temperature, ε the surface emissivity, C_p the specific heat of the undercooled melt, and σ_{SB} the Stefan-Boltzmann constant. For the Al-Mn alloys, we take values of $\rho=3.26$ g/cm^3,[22] $T_R=300$ K, and $\varepsilon=0.1$ as an approximation from experimentally determined values for liquid aluminum.[23] As an estimate, we use the value $C_p=1.1$ J/(g K) for the specific heat of an Al-Cu-V liquid.[7] Using these values and solving Eq. (1) allows for a quantitative calculation of the cooling rate as a function of droplet diameter.

A gas-atomizing facility has been applied to extend the experiments toward droplets smaller than 100 μm, the minimum size for the drop-tube-processed particles. The ingot sample was placed into a glassy crucible and melted by a resistance furnace. Subsequently, the molten sample was pressed through a thin nozzle (0.5 mm in diameter) with argon gas at a pressure of 100 kPa. Immediately below the nozzle, the melt is atomized by helium flowing through a concentric-ring nozzle at a pressure of 1 MPa. Droplets in diameter of 20–60 μm were obtained in this way. Further details of the atomizing facility are given elsewhere.[24]

All of the solidified droplets were separated into size fractions by sieving with standard meshes. The microstructures and phases formed in the as-solidified droplets of the various size groups were investigated by x-ray investigations using Cu $K\alpha$ radiation, optical, scanning, and transmission electron microscopy including energy dispersive x-ray analysis (EDX), and differential scanning calorimetry (DSC II, Perkin-Elmer).

Samples for transmission electron microscopy were prepared by mixing the droplets with glue. The glue was cast into a brass tube (diameter 3 mm) and heated to about 150° for hardening. Subsequently, the tube was cut into thin slices which were mechanically ground, dimpled, and ion milled to perforation in a stage cooled by liquid nitrogen. The samples were investigated in a JEOL 2000 EX electron microscope.

III. EXPERIMENTAL RESULTS

In the drop-tube experiments, droplets in size between 100 and 1000 μm are prepared, which solidify during the free-fall period in a containerless state. Droplets larger than 1 mm are still liquid when touching the bottom of the drop tube. They are splattered onto a Cu substrate and form thin foils of thickness of approximately 150 μm. By solving the boundary problem of Eq. (1) for a total fall time of 0.55 s, we arrive at a minimum undercooling in the range of 150–200 K.[13] It is interesting to note that splattering such droplets from the state of an undercooled melt leads to the formation of single T-phase samples,[13] which could not be obtained otherwise by, e.g., melt spinning from temperatures above the liquidus temperatures of the alloy.[1,15–18]

As an example, Fig. 1 shows a scanning electron micrograph of a section through an $Al_{88}Mn_{12}$ droplet from the 0.8–0.9-mm size fraction. Two different phases are apparent: a very pronounced dendritic microstructure of a Mn-rich phase 14–22 at. % Mn, which is embedded in a supersaturated Al_{SS} solid solution ($\approx$2.5 at. % Mn).

Figure 2 gives an x-ray-diffraction pattern for $Al_{88}Mn_{12}$ droplets of size group 0.8–0.9 mm. In these droplets the intermetallic phase Al_6Mn, Al_{SS}, and the quasicrystalline T phase are apparent. Heating the smaller droplets to a temperature of 880 K leads to a complete transformation of the metastable T phase into the equilibrium phase Al_6Mn (not shown). These findings suggest that the formation of T phase is competing with the formation of Al_6Mn.[13]

Figure 3 shows a TEM image of decagonal quasicrystals in droplets of the same size fraction as shown in Fig. 1. The inset of Fig. 3 represents an electron-diffraction pattern from the decagonal phase of the same droplet taken with the incident electron beam parallel to the tenfold zone axis. The TEM measurements clearly reveal

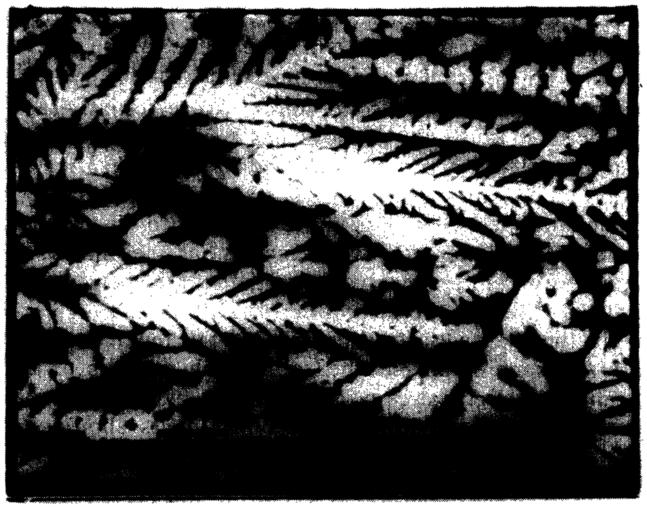

FIG. 1. Scanning electron micrograph of a section through an $Al_{88}Mn_{12}$ droplet of 0.8 mm diameter. Two different phases are apparent: a very pronounced dendritic microstructure of a Mn-rich phase (14–22 at. % Mn), which is embedded within a supersaturated Al_{SS} solid solution (2.5 at. % Mn).

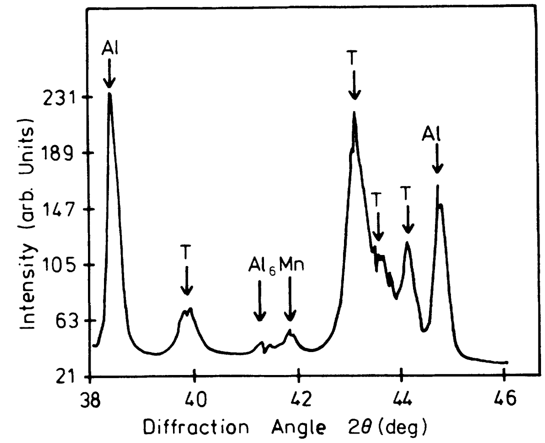

FIG. 2. X-ray-diffraction pattern for $Al_{88}Mn_{12}$ droplets of size group 0.8–0.9 mm. In these droplets intermetallic phase Al_6Mn, supersaturated Al_{SS}, and quasicrystalline T phase have been detected.

the existence of the quasicrystalline T phase. However, the quasicrystalline I phase could not be detected even in the smallest droplets processed in the drop tube.

The atomization facility leads to an extension of the droplet size toward smaller droplets in the range of 60–20 μm diameter. In contrast to the drop-tube-processed droplets, the atomized samples contain both quasicrystalline phases, the T and I phases. No equilibrium phases could be identified in the atomized droplets by x-ray diffraction. The fraction of I phase increases with decreasing droplet diameter at the expense of the T phase.[25]

In order to determine the volume fractions of the respective metastable quasicrystalline phases in the droplets of the various size groups, DSC investigations and image processing in combination with scanning electron microscopy (SEM) were utilized. DSC experiments on splats of single T-phase samples record the heat of crystallization as the metastable T phase transforms into the equilibrium Al_6Mn phase ($\Delta H_x^r = 24$ kJ/mol), in agreement with previous results.[19] This value gives a reference point for the determination of the mass fraction X of the quasicrystalline phase, which is inferred from $X = \Delta H_x(d)/\Delta H_x^r$. Here $\Delta H_x(d)$ corresponds to the heat of crystallization as measured by DSC experiments on the droplets of the various size groups of diameter d.

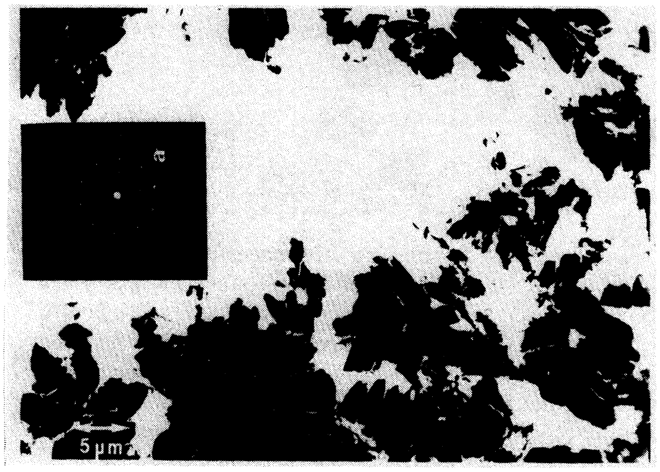

FIG. 3. Transmission-electron-microscopy image of dodecagonal quasicrystals in droplets of the same size fraction as shown in Fig. 1. The inset represents an electron-diffraction pattern from the dodecagonal phase of the same droplet taken with the incident electron beam perpendicular to the tenfold zone axis.

The results of these investigations are shown in Fig. 4, where the mass fraction of the different phases, X, is plotted as a function of the droplet diameter d. The upper ordinate gives the cooling rate $\dot{T}$ as a function of droplet diameter d according to the calculations using Eq. (1). Figure 4 represents a contour map of the different phases formed in undercooled $Al_{88}Mn_{12}$ droplets of various size groups containerlessly processed. The open circles give the results of the volume fraction of the metastable T phase as measured by DSC in the drop-tube-processed samples with the bars marking the uncertainty of these measurements. The solid squares characterize the results obtained by image-processed SEM. The open squares correspond to the volume fractions as measured by x-ray diffraction. For comparison, the solid circle on the right-hand side of Fig. 4 corresponds to the phase distribution in $Al_{88}Mn_{12}$ if the melt solidifies under equilibrium conditions. For two droplet-size groups of mean diameter $\bar{d} = 800$ and 125 μm, the Mn concentration in the supersaturated solid solution Al_{SS} has been measured by EDX. The results are indicated by the arrows in Fig. 4 exhibiting a Mn content in Al_{SS} of 2.5 at. % for the 800-μm droplets and of about 4 at. % for the 125-μm droplets, respectively.[25] The dashed line in the right-hand side of Fig. 4 separating the Al_6Mn phase from the supersaturated solid solution Al_{SS} is based on an analysis of x-ray-diffraction experiments. The dashed line on the left-hand side gives the separation of T and I phases as investigated by x-ray and DSC measurements on the atomized particles. However, these results should be regarded as semiquantitative only, with relatively high uncertainty. The reason is that the measurements were performed on small sample masses because of the scarce output of very refined powder in the atomization experiments.

From Fig. 4 critical cooling rates $\dot{T}_c$ necessary for the avoidance of formation of the crystalline phases in the undercooled $Al_{88}Mn_{12}$ melts are deduced. Apparently, a critical cooling rate of approximately 1000 K/s is necessary to circumvent the crystallization of the stable intermetallic phase Al_6Mn. On the other hand, Fig. 4 shows that the formation of the quasicrystalline T phase takes place even at moderate cooling rates, while the crystallization of the quasicrystalline I phase needs cooling rates exceeding 1×10^4 K/s. The solid and open triangles represent results of the formation of the T phase obtained in previous investigations on the same alloy system applying drop-tube processing[25] and droplet-dispersion technique,[26] respectively.

For comparison, surface-melting experiments on Al-Mn alloys by electron-beam heating indicated that stable intermetallic Al_6Mn was formed at slow electron-beam-scan velocities of 0.25 cm/s. The maximum growth velocity of this phase in Al-Mn alloys was determined to be

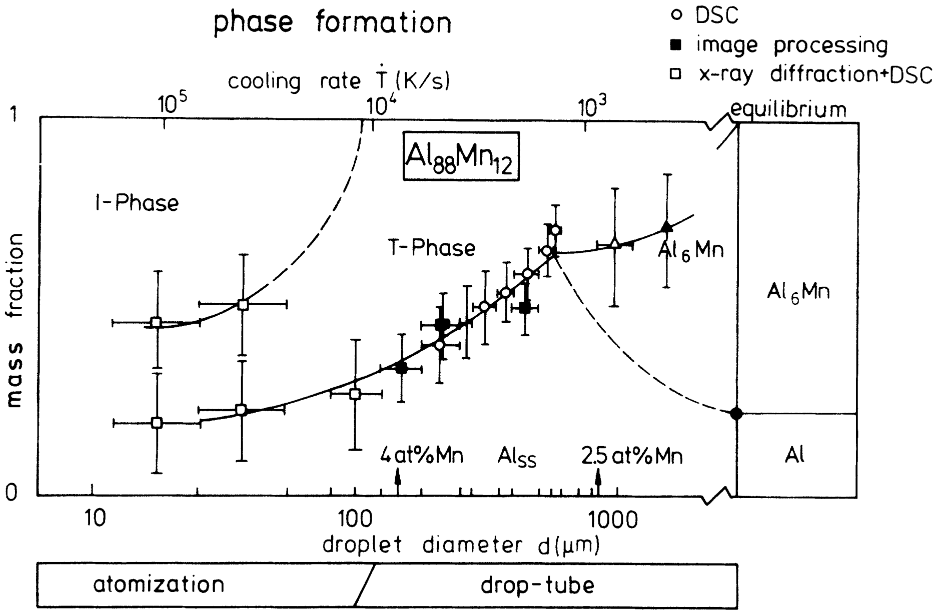

FIG. 4. Phase-selection diagram showing the mass fraction X of various phases formed during containerless solidification of droplets of $Al_{88}Mn_{12}$ as a function of droplet diameter d. The open circles give the results of the mass fraction of the metastable T phase as inferred from DSC measurements. The solid squares characterize the results obtained by image processing in the SEM. The open squares represent results by x-ray-diffraction and DSC experiments. For comparison, the open and solid triangles give results of previous work applying drop-tube processing (Ref. 25) and the droplet-dispersion technique (Ref. 26). The right-hand side corresponds to the phase distribution if equilibrium solidification is assumed. The upper ordinate exhibits the cooling rates deduced from thermal-balance calculations according to Eq. (1). The arrows mark the Mn concentrations in supersaturated Al_{SS} as measured by EDX in SEM experiments.

in the range of 1–2.5 cm/s.[27] An increase of the scan velocity establishes an undercooling ahead of the crystalline phases growing from the substrate. This leads first to the occurrence of the quasicrystalline T phase and, with further increasing scan velocity, to the development of the quasicrystalline I phase. The analysis of the as-solidified microstructures indicates that at high scan velocities the icosahedral dendrites retain their icosahedral structure, but at low scan rates they are replaced by the T phase epitaxially grown onto the primarily formed I phase. On the other hand, Eady, Hogan, and Davies[28] have developed a relation between the maximum growth velocity of Al_6Mn in Al-Mn melts and the concentration yielding $U_{max} \approx 0.25$ cm/s for $Al_{88}Mn_{12}$.

Other electron- and laser-beam melting experiments on Al-Mn alloys reveal that the icosahedral phase is stable against transformation to the T phase for at least 200 μs at 933 K. A minimum cooling rate of 1×10^6 K/s has been suggested to suppress the formation of the T phase.[29]

IV. THEORETICAL ANALYSIS OF NUCLEATION AND PHASE FORMATION

The description of the transformation behavior of undercooled Al-Mn melts requires knowledge of the driving force for phase formation, ΔG_v, the activation energy for nucleation, ΔG^*, the nucleation frequency I_{SS}, and the crystal-growth velocity U of the respective phases involved in the solidification of the undercooled melt in order to develop the full transformation kinetics.

A. Free-energy difference between solid and liquid

Following simple thermodynamic considerations, the difference of the free energy between solid and liquid, ΔG_v, reads

$$\Delta G_v = \Delta H - T\,\Delta S \ , \tag{2a}$$

with

$$\Delta H = \Delta H_f - \int_T^{T_L} \Delta C_p \, dT \tag{2b}$$

and

$$\Delta S = \Delta S_f - \int_T^{T_L} \Delta C_p \frac{dT}{T} \ . \tag{2c}$$

Here ΔH and ΔS denote the differences of the enthalpies and entropies of the liquid and solid states, respectively. $\Delta S_f = \Delta H_f / T_L$ is the entropy of fusion, ΔH_f the heat of fusion, and ΔC_p the difference of the specific heat between liquid and solid states. Provided experimental values for the heat of fusion and the specific heats in both the undercooled melt regime and the solid state are available, the free-energy difference ΔG_v can be calculated as a function of temperature from Eq. (2a). So far, no reliable measurements of the specific heat in undercooled Al-Mn alloys have been reported. However, very recently measurements of the specific heat in the liquid, amorphous, and icosahedral states of Al-Cu-V alloys have been pub-

TABLE I. Characteristic thermodynamic data used for the calculations of the transformation behavior of the undercooled melt into intermetallic Al_6Mn, supersaturated Al_{SS}, and T and I phases, respectively.

Parameter	Units	Al_6Mn	Al	T phase	I phase
Liquidus temperature	K	1193[a]	933[a]	1136[b]	1081[b]
Glass temperature	K	615	225[c]	658[d]	658[d]
Mole weight	g/mol	30.3	27.0	31.2	31.2
Entropy of fusion	J/K mol)	10.4[a]	11.56[a]	8.45[d]	8.42[d]
α		0.86	0.86	0.45	0.36
$f(\vartheta)$		0.15	0.12	1.00	1.00
A	K	2485	1504	2106[d]	2106[d]
η_0	10^{-2} P	4.120	1.644	1.221	0.688
ξ		10^{-10}	10^{-6}	1	1
Mass density	g/cm^3	3.35	2.7	3.29[e]	3.29[e]

[a] Experimentally determined.
[b] Taken from Ref. 34.
[c] Taken from Ref. 39.
[d] Taken from Ref. 35.
[e] Taken from Ref. 22.

lished.[7] Assuming that the data of the liquid can be extrapolated into the regime of the undercooled melt, the free-energy difference ΔG_v can be evaluated for this alloy. A comparison of such calculations with presently available models[30-33] for the description of the temperature dependence of ΔG_v gives the best agreement if an expression is used as applied earlier for the description of phase formation in undercooled Al-Mn melts:[14]

$$\Delta G_v = \Delta S_f \Delta T - \gamma\, \Delta S\left[\Delta T - T\ln\left[\frac{T_L}{T}\right]\right], \tag{3}$$

with $\gamma=[\ln(T_L/T_0)]^{-1}$ a proportionality constant. For the estimation of the free-energy difference between undercooled Al-Mn alloys and the respective solid phases under consideration, we apply Eq. (3), using values for the entropy of fusion ΔS_f and the ideal glass temperatures T_0 as given in Table I. The melting temperatures of quasicrystalline I and T phases have been measured by laser-pulse heating experiments on Al-Mn alloys.[34] The equivalent data are also collected in Table I. On the basis of these data, the free-energy differences were calculated for the formation of stable intermetallic Al_6Mn, Al phase, and the quasicrystalline I and T phases. The results are shown in Fig. 5. For all phases, ΔG_v decreases monotonically with increasing temperature T, leading to intersection points with the ordinate ($\Delta G_v=0$) at the respective melting temperatures of the various phases. The $\Delta G_v(T)$ curve for intermetallic Al_6Mn is based upon values of ΔS_f and T_L as determined experimentally by differential thermal analysis (DTA), whereas the corresponding curves for the quasicrystalline phases are the same as previously calculated by Battezati, Antonione, and Marino[35] using the experimentally measured virtual melting temperatures of the metastable I and T phases.[34]

B. Activation energy for nucleation

According to classical nucleation theory, the activation threshold ΔG^* for the formation of a critical nucleus is given by[6]

$$\Delta G^* = \frac{16\pi\sigma^3}{3\,\Delta G_v^2} f(\vartheta)\ . \tag{4}$$

Here σ is the interfacial energy of the solid-liquid interface and $f(\vartheta)$ is the catalytic potency factor for heterogeneous nucleation, which depends on the wetting angle ϑ. The most decisive parameter is the interfacial energy σ. To estimate σ for the various phases, we refer to the negentropic model developed by Spaepen[8] and Thompson:[8,36]

$$\sigma = \alpha\frac{\Delta S_f T}{(N_L V_m^2)^{1/3}}\ , \tag{5}$$

where α is a factor depending on the structure of the solid nucleus, N_L is Avogadro's number, and V_m is the

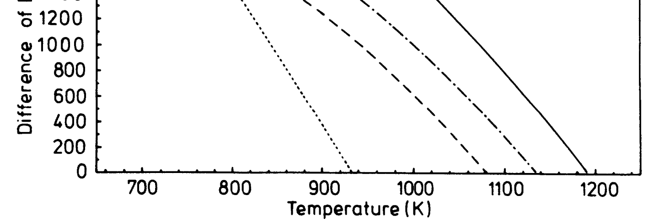

FIG. 5. Free-energy difference ΔG_v as a function of temperature for intermetallic Al_6Mn, the supersaturated Al_{SS} solid solution, and the quasicrystalline T and I phases, respectively.

molar volume. For the calculations we use $\alpha = 0.86$ for the nucleation of the Al_6Mn and Al phases, and $\alpha = 0.45$ and 0.36 for the quasicrystalline T and I phases, respectively. Even though these values are chosen somewhat arbitrarily, the sequence of magnitude should be in the right order. The negentropic model delivers $\alpha = 0.86$ for fcc structure, hence a suitable value for Al_6Mn and Al. The structure factor is expected to decrease in the case of the quasicrystalline phases (see Introduction), whereby the three-dimensional icosahedral phase should have the lowest value of the interface energy. The temperature dependence of ΔG^* is calculated supposing homogeneous nucleation for the quasicrystalline phases as they are likely in the drop-tube experiments and, alternatively, heterogeneous nucleation for the formation of the crystalline phases of Al_6Mn and Al with a catalytic potency factor $f(\vartheta) = 0.15$ and 0.12, respectively, and using the results of Fig. 5. The results are shown in Fig. 6. According to these considerations, the heterogeneous nucleation of Al_6Mn is preferred at moderate undercooling temperatures. However, if the undercooling increases approaching the range of $\Delta T \approx 150-200$ K, the activation energies for the nucleation of Al_6Mn, the T and I phases become comparable. The calculation of the activation energies for nucleation gives the basis for the estimation of the nucleation rates.

C. Nucleation frequency

Following the work of Turnbull,[37] the steady-state homogeneous nucleation rate I_{SS} is given by

$$I_{SS} = \frac{k_B T N_n}{3\eta(T) a_0^3} \exp\left[-\frac{\Delta G^* f(\vartheta)}{k_B T} \right] . \tag{6}$$

Here a_0 denotes a typical interatomic spacing and $\eta(T)$ represents the viscosity of the undercooled melt. N_n measures the number of potential nucleation sites. In the case of homogeneous nucleation, it equals Avogadro's number N_L, while for heterogeneous nucleation it is reduced since only atoms at the interface to the heterogeneous catalytic site can be the origin of a nucleus. This is regarded by the relation $N_n = \xi N_L$, where $\xi \ll 1$ represents the fraction of atoms which can act as an origin of a heterogeneous nucleus, while $\xi = 1$ describes the homogeneous case. If the heterogeneous nucleation at the surface of the droplets is assumed, only atoms at the surface can act as nucleation sides. In this case the ratio ξ approaches values of $\xi = 10^{-10}$ and 10^{-6} for Al_{SS} and Al_6Mn, respectively.

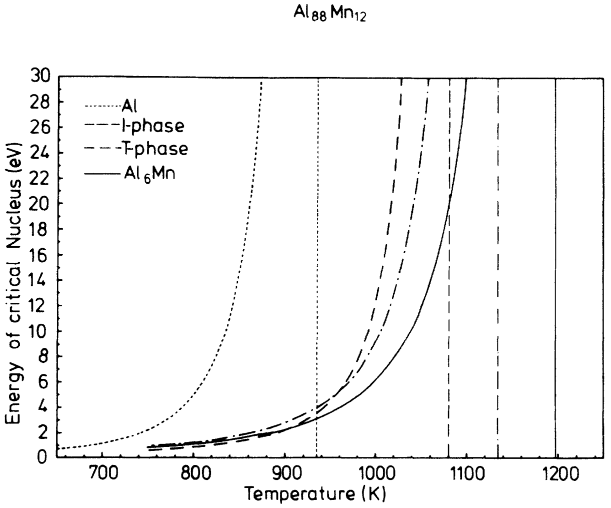

FIG. 6. Activation energy for the formation of critical nuclei as a function of temperature for intermetallic Al_6Mn, the supersaturated Al_{SS} solid solution, and the quasicrystalline T and I phases, respectively. The vertical lines correspond to the liquidus temperatures of the respective phases.

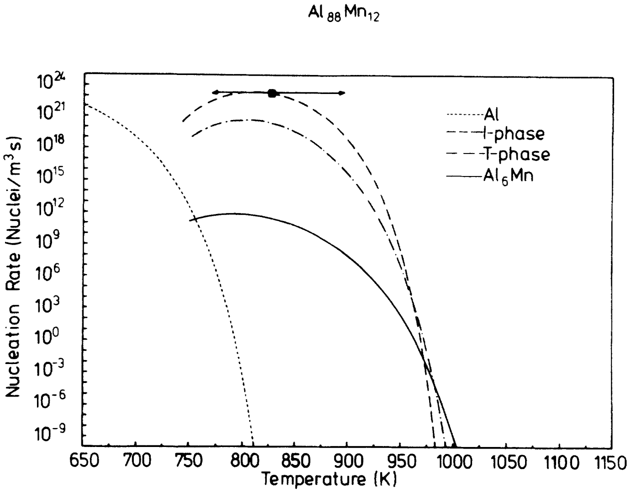

FIG. 7. Steady-state nucleation rate I_{SS} as a function of temperature for intermetallic Al_6Mn, the supersaturated Al_{SS} solid solution, and the quasicrystalline T and I phases, respectively. The solid square represents the maximum nucleation rate as inferred from atomization experiments (Ref. 12).

In order to determine the viscosity, we use a Vogel-Fulscher-Tammann expression for Al-Mn alloys:[34]

$$\eta(T) = \eta_0 \exp\left[\frac{A}{T - T_0} \right] . \tag{7}$$

To evaluate the parameters of A and η_0, we refer to the work by Battezzati, Antonione, and Marino.[35] Further on, we assume a viscosity of $\eta(\mathrm{Al}) \approx 10^{-1}$ P and $\eta(\mathrm{Al_6Mn}) \approx 10^{0}$ P at the melting temperature as typical values for a metal and an alloy, respectively.

Values of A, η_0, T_0, $f(\vartheta)$, and ξ used for the calculations of the nucleation rates of the various phases under consideration are given in Table I.

Figure 7 gives the nucleation rates as a function of temperature for the different phases. The results suggest that at moderate undercooling the nucleation rate of the intermetallic phase Al_6Mn is predominant, whereas at larger undercooling the nucleation of the quasicrystalline phases becomes more likely. In the case of homogeneous nucleation of the I phase, the results of the calculations indicate a maximum nucleation rate of approximately $I_{SS}(\max) = 10^{22}\ \mathrm{m^{-3}\,s^{-1}}$, which is in fair agreement with experimental results of the density of quasicrystalline nanocrystallites in electrohydrodynamically atomized

Al-Mn powders.[12] This is shown by the solid square in Fig. 7, which has been calculated taking into account the density of quasicrystallites in the atomized powders and the cooling conditions in these experiments.

D. Crystal-growth velocity

The crystal-growth velocity U is determined using the expression for diffusion-controlled growth of a planar rough interface,[6]

$$U=\frac{D}{a_0}\left[1-\exp\left[\frac{\Delta G_v}{k_B T}\right]\right], \tag{8}$$

where D is the diffusion coefficient which is correlated to the viscosity via the Einstein-Stokes relation $D=(k_B T)/(3\eta a_0)$. Taking into account the results of Fig. 5, the crystal-growth rate U has been calculated and the results are shown in Fig. 8. At low temperatures no essential differences in the growth behavior of the different phases is found, whereas at higher temperatures the computed curves suggest that the Al_6Mn phase grows more sluggish than the quasicrystalline phases. In particular, maximum growth velocities in the range of $U \approx 1$ and 2.5 cm/s are predicted by the calculations for the various phases, which are in agreement with values experimentally determined by electron-beam-heating experiments on Al-Mn alloys.[27]

E. Temperature–time-transformation diagram

The temperature–time-transformation (TTT) curves are calculated for all phases considered here on the basis of the above-discussed nucleation and crystal-growth behavior. The time t necessary to produce a mass fraction $X=10^{-3}$, which is barely detectable by the applied techniques, of the equivalent phases formed at a certain undercooling is given by[38]

$$X=I_{SS}U^3t^4 . \tag{9}$$

Figure 9 summarizes the TTT diagrams for the crystalline phases of Al_6Mn and Al. Corresponding TTT curves for the quasicrystalline T and I phases are given as well. The TTT curves suggest an achievable undercooling of approximately 150–200 K. This matches quite well the experimentally estimated undercoolings of the present drop-tube measurements (see Sec. II). The TTT curves predict a sequence of phase formation with the cooling rate under the conditions of containerlessly processed droplets and particles in a high-purity environment. At small cooling rates, Al_6Mn intermetallic and crystalline Al preferably solidify. Faster cooling leads to the progressively increasing mass fraction of the quasicrystalline T phase at the expense of Al_6Mn. At cooling rates larger than $\dot{T}=1000$ K/s, the intermetallic phase Al_6Mn disappears, while the quasicrystalline T phase should progressively form. Further increasing the cooling rate to 1×10^4 K/s leads to the crystallization of the quasicrystalline I phase, in agreement with the experimental findings. In order to avoid the nucleation of quasicrystalline phases, cooling rates larger than 10^6 K/s are required. This finding explains the observation that Al-Mn alloys cannot be prepared in an amorphous structure by melt spinning or splat cooling, which provide maximum cooling rates in the order of maximum 10^6 K/s.

V. SUMMARY AND CONCLUSIONS

Phase-selection processes have been investigated in Al-Mn droplets undercooled and solidified containerlessly in a drop tube and an atomization facility. A contour map has been developed which gives the mass fractions of

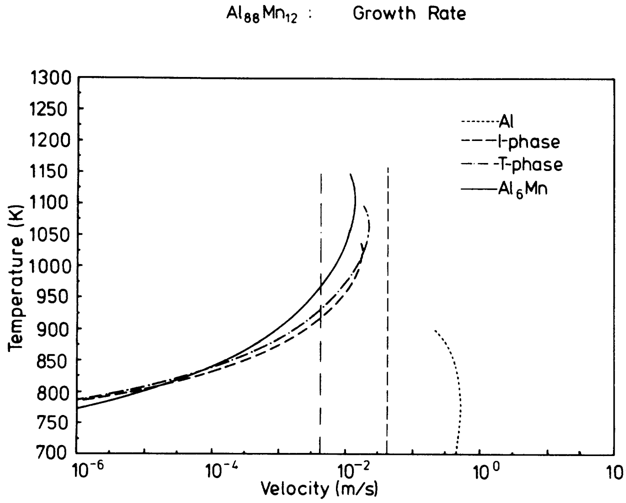

FIG. 8. Crystal-growth velocity U as a function of temperature for intermetallic Al_6Mn, the supersaturated Al_{SS} solid solution, and the quasicrystalline T and I phases, respectively. The vertical lines give the range of maximum growth velocities as suggested by previous work (Refs. 27 and 28).

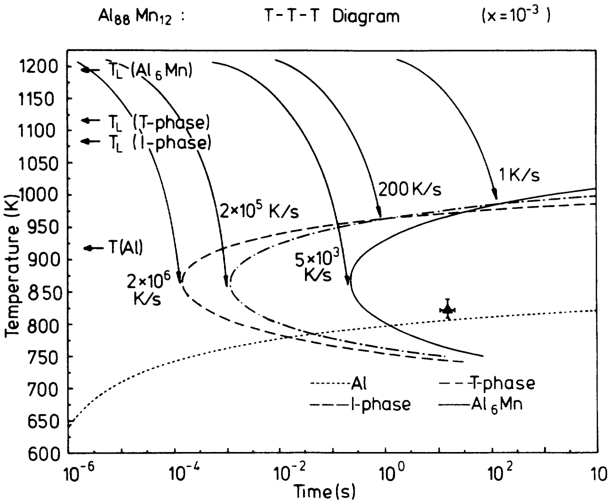

FIG. 9. Temperature–time-transformation diagrams of the various phases involved in the solidification of undercooled droplets of $Al_{88}Mn_{12}$ assuming a fixed volume fraction of $X=10^{-3}$. Critical cooling rates are also shown for the avoidance of crystallization of various phases. The solid triangle corresponds to the maximum undercoolability of the Al phase in Al-Mn alloys as investigated by the droplet-dispersion technique (Ref. 26).

phases formed in the droplets as a function of droplet diameter. The droplet diameter has been correlated with the cooling rates on the basis of thermal-balance calculations of the freely falling samples. These results allow the study of the phase-formation kinetics with respect to the solidification of stable crystalline intermetallic Al_6Mn, supersaturated Al_{SS}, and the quasicrystalline dodecagonal and icosahedric phases.

The experimental findings have been discussed within classical nucleation theory in terms of nucleation rate, crystal growth, and transformation rate. On the basis of thermodynamic parameters of undercooled Al-Mn melts, the free-energy difference ΔG_v, the activation energy for the formation of critical nuclei ΔG^*, and the crystal-growth velocity U have been calculated as a function of undercooling for all of the phases of interest in the solidification behavior of Al-Mn melts. Using the results of such calculations, the transformation kinetics has been developed, leading to full time–temperature-transformation diagrams for intermetallic Al_6Mn, supersaturated Al_{SS}, and quasicrystalline dodecagonal T and icosahedral I phases. The TTT curves are in agreement with the experimentally determined phase evolution in droplets containerlessly processed in a drop tube and in an atomization facility. They correlate well with the experimentally observed phase-selection behavior as a function of droplet diameter or the cooling rate.

ACKNOWLEDGMENTS

The authors want to thank B. Feuerbacher for continuous support, stimulating discussions, and a careful reading of the manuscript and H. Mühlmeyer and H. Grill for technical assistance. Also, useful discussions with J. Kreis are gratefully acknowledged.

---

[1] D. Shechtman, I. Blech, D. Gratias, and J. W. Cahn, Phys. Rev. Lett. **53**, 1951 (1984).
[2] L. A. Bendersky, Phys. Rev. Lett. **55**, 1461 (1985).
[3] M. D. Ball and D. J. Lloyd, Scr. Metall. **19**, 1065 (1985).
[4] A. P. Tsai, A. Inoue, and T. Masumoto, Jpn. J. Appl. Phys. **26**, L1505 (1987).
[5] W. Ohashi and F. Spaepen, Nature **330**, 555 (1987).
[6] J. W. Christian, *The Theory of Transformation in Metals and Alloys* (Pergamon, Oxford, 1975).
[7] J. C. Holzer and K. F. Kelton, Acta Metall. **39**, 1833 (1991).
[8] F. Spaepen, Acta Metall. **23**, 729 (1975).
[9] F. C. Frank, Proc. R. Soc. London A **215**, 43 (1952).
[10] P. J. Steinhardt, D. R. Nelson, and M. Ronchetti, Phys. Rev. B **28**, 784 (1983).
[11] D. R. Nelson and F. Spaepen, Solid State Phys. **42**, 1 (1989).
[12] R. J. Schäfer, L. A. Bendersky, and F. S. Biancanillo, J. Phys. (Paris) Colloq. **47**, C3-311 (1986).
[13] J. Kreis, D. M. Herlach, H. Alexander, and W. Weiss, J. Non-Cryst. Solids **117/118**, 816 (1990).
[14] F. Gillessen and D. M. Herlach, Mater. Sci. Eng. A **134**, 1220 (1991).
[15] D. Shechtman and I. Blech, Metall. Trans. A **16**, 1005 (1985).
[16] L. Bendersky, R. F. Schaefer, F. S. Biancaniello, W. J. Boettinger, M. J. Kaufmann, and D. Shechtman, Scr. Metall. **19**, 909 (1985).
[17] L. A. Bendersky and S. D. Ridder, J. Mater. Res. **1**, 1 (1986).
[18] R. J. Schaefer, L. Bendersky, D. Shechtman, W. J. Boettinger, and F. S. Biancaniello, Metall. Trans. A **17**, 2117 (1986).
[19] K. F. Kelton and J. C. Holzer, Phys. Rev. B **37**, 3940 (1988).
[20] F. Gillessen and D. M. Herlach, Mater. Sci. Eng. **97**, 147 (1988).
[21] R. B. Bird, W. E. Stewart, and E. N. Lightfood, *Transport Phenomena* (Wiley, New York, 1960).
[22] K. F. Kelton and T. W. Wu, Appl. Phys. Lett. **46**, 1059 (1985).
[23] J. K. R. Weber and R. A. Schiffmann (unpublished).
[24] N. Uebber and L. Ratke, Scr. Metall. **25**, 1133 (1991).
[25] J. Kreis and D. M. Herlach (unpublished).
[26] B. A. Mueller, R. J. Schaefer, and J. H. Perepezko, J. Mater. Res. **2**, 809 (1987).
[27] R. J. Schaefer and L. A. Bendersky, in *Rapidly Solidified Alloys and Their Mechanical and Magnetic Properties,* edited by B. C. Giessen, D. E. Polk, and A. I. Taub, MRS Symposia Proceedings No. 58 (Materials Research Society, Pittsburgh, 1986), p. 217.
[28] J. A. Eady, L. M. Hogan, and P. G. Davies, J. Aust. Inst. Met. **20**, 23 (1975).
[29] D. M. Follstaedt and J. A. Knapp, in *Rapidly Solidified Alloys and Their Mechanical and Magnetic Properties* (Ref. 27), p. 233.
[30] D. Turnbull, J. Chem. Phys. **20**, 411 (1952).
[31] C. V. Thompson and F. Spaepen, Acta Metall. **27**, 1855 (1979).
[32] K. S. Dubey and P. Ramachandrarao, Acta Metall. **32**, 91 (1984).
[33] L. Battezzati and E. Garrone, Z. Metallkd. **75**, 305 (1984).
[34] J. A. Knapp and D. M. Follstaedt, Phys. Rev. Lett. **58**, 2454 (1987).
[35] L. Battezzati, C. Antonione, and F. Marino, J. Mater. Sci. **24**, 2324 (1989).
[36] C. V. Thompson, Ph.D thesis, Harvard University, 1979.
[37] D. Turnbull, Contemp. Phys. **10**, 473 (1969).
[38] M. Avrami, J. Chem. Phys. **7**, 1103 (1939).
[39] H. J. Fecht and W. J. Johnson, Nature (London) **324**, 50 (1988).

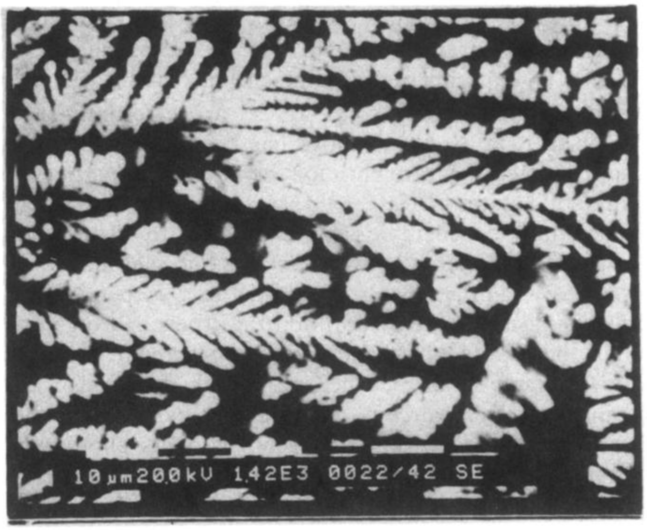

FIG. 1. Scanning electron micrograph of a section through an $Al_{88}Mn_{12}$ droplet of 0.8 mm diameter. Two different phases are apparent: a very pronounced dendritic microstructure of a Mn-rich phase (14–22 at. % Mn), which is embedded within a supersaturated Al_{SS} solid solution (2.5 at. % Mn).

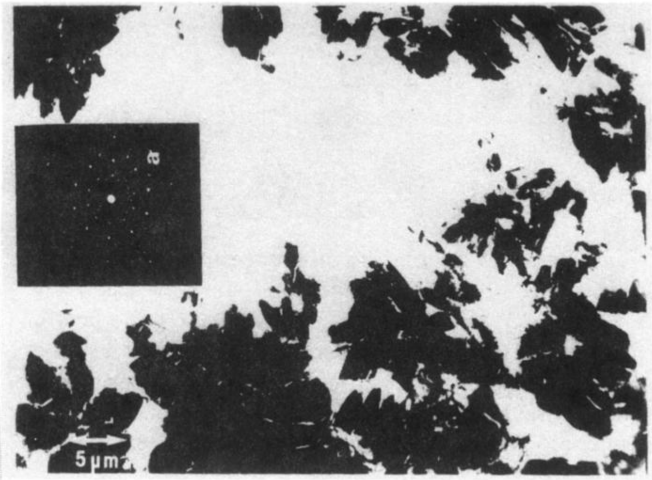

FIG. 3. Transmission-electron-microscopy image of dodecagonal quasicrystals in droplets of the same size fraction as shown in Fig. 1. The inset represents an electron-diffraction pattern from the dodecagonal phase of the same droplet taken with the incident electron beam perpendicular to the tenfold zone axis.